Anomalous viscosity effect in the early stages of the ion-assisted adhesion/fusion event between lipid bilayers

Raudino, Antonio; Marrink, Siewert J.; Pannuzzo, Martina

Published in:
Journal of Chemical Physics

DOI:
10.1063/1.4809993

Anomalous viscosity effect in the early stages of the ion-assisted adhesion/fusion event between lipid bilayers: A theoretical and computational study

Antonio Raudino,[1,a)] Siewert J. Marrink,[2] and Martina Pannuzzo[3]
[1]*Dipartimento di Scienze Chimiche, Università di Catania, Viale A. Doria 6, 95125 Catania, Italy*
[2]*Dept of Biophysical Chemistry, University of Groningen, Nijenborgh 4, 9747 AG Groningen, The Netherlands*
[3]*Dept of Computational Biology, Universität Erlangen-Nürnberg, Staudtstr.5, 91058 Erlangen, Germany*

(Received 28 January 2013; accepted 13 May 2013; published online 17 June 2013)

The effect of viscosity on the encounter rate of two interacting membranes was investigated by combining a non-equilibrium Fokker-Planck model together with extensive Molecular Dynamics (MD) calculations. The encounter probability and stabilization of transient contact points represent the preliminary steps toward short-range adhesion and fusion of lipid leaflets. To strengthen our analytical model, we used a Coarse Grained MD method to follow the behavior of two charged palmitoyl oleoyl phosphatidylglycerol membranes embedded in a electrolyte-containing box at different viscosity regimes. Solvent friction was modulated by varying the concentration of a neutral, water-soluble polymer, polyethylene glycol, while contact points were stabilized by divalent ions that form bridges among juxtaposed membranes. While a naïve picture foresees a monotonous decrease of the membranes encounter rate with solvent viscosity, both the analytical model and MD simulations show a complex behavior. Under particular conditions, the encounter rate could exhibit a maximum at a critical viscosity value or for a critical concentration of bridging ions. These results seem to be confirmed by experimental observations taken from the literature. © *2013 AIP Publishing LLC*. [http://dx.doi.org/10.1063/1.4809993]

I. INTRODUCTION AND MOTIVATION OF THE PAPER

Membrane adhesion and fusion are ubiquitous and fundamental processes in biological systems. Cells use them to transport material both between intracellular compartments and out of cells: this is the typical mechanism, e.g., for hormone secretion and for vesicle mediated synaptic transmission.

Several chemical substances have an influence on the fusion rate. Most of them (from different kinds of membrane-anchored proteins to simple divalent cations) form tight ligand-receptor pairs between nearby membranes bringing them to contact distance.

Addition of uncharged water-soluble polymers that do not appreciably interact with the vesicles' surfaces may dramatically enhance the adhesion/fusion rate. The most common one is the polyethylene glycol (PEG), but also other polymers (e.g., dextran) show a comparable behavior. The contemporary presence of bridging compounds (e.g., divalent cations), and neutral hydrophilic polymers exerts a synergistic effect on the fusion rate of charged lamellar vesicles.[1] It is commonly thought that the polymer effect is mainly due to osmotic forces originating from the entropy-driven exclusion of the flexible polymer chains from the inter-bilayer spacing.[2] Recently, analytical models and extensive Molecular Dynamics (MD) simulations performed by us evidenced the role of the excess of ions near the membrane-water interface in excluding low dielectric permittivity polymer chains from the inter-lamellar spacing.[3]

On the experimental side, most of fusion assays have been performed by varying the calcium concentration while keeping constant the polymer fraction ϕ.[1] These studies had found a dramatic increase of the fusion rate upon polymer addition once a critical threshold of calcium ions has been reached. Other viscosity enhancers like sucrose have a similar effect on the fusion rate.[4] Fewer works investigated the fusion rate by varying the polymer concentration ϕ and just a few investigated the effect of the polymer chain length N by maintaining constant both polymer and calcium concentration.[5] As far as the adhesion process alone is considered (those not followed by adhering bilayers fusion), other authors observed an effect of the polymer length similar to that of the fusion rate.[6]

Experiments performed by varying the polymer length N are far more interesting than those performed by varying the polymer concentration ϕ. Indeed, solvent properties such as polarity, polymer-solvent miscibility, and surface tension do not significantly change with polymer length (they depend on polymer length as N^{-1}, then the effect is negligible when $N \gg 1$) while they do depend on ϕ. On the contrary, solution viscosity ω sharply increases with N and ϕ (in dilute solutions the effect is less evident:[7] $\omega \approx \omega|_{\phi=0}(1 + |C|N^{1/2}\phi)$, but for entangled chains the viscosity increase is dramatic:[8] $\omega \approx N^3\phi^{3/2}$. Whence, we conclude that experiments performed by changing the polymer length (while keeping constant the polymer concentration) mainly describe the effects of the altered viscosity alone. Because of PEG-enhanced viscosity, the favorable effect of PEG on the fusion rate could

a)E-mail: araudino@dipchi.unict.it

be related to osmotic forces partially balancing the viscosity-dependent decrease of the encounters probability among lipid vesicles.

The above experiments, either those performed at constant ϕ or, more importantly, those performed by varying the chain length N, evidence a maximum in the fusion rate on increasing solvent friction. The occurrence of a maximum could reflect a balance between augmented osmotic forces and reduced encounter probability, however, as discussed below, other scenarios are worth exploring.

The anomalous effect of solvent friction on the reaction rate is not at all a new field. While most molecular systems exhibit a decrease of the rate on increasing solvent viscosity, some interesting cases showing an opposite behavior have been reported over the years.[9]

From a theoretical standpoint, this ambivalent friction behavior has been foreseen long time ago by Kramers[10] who investigated the escape problem of a particle of mass m from a potential well under the effect of a random white noise and a solvent friction $\Gamma \equiv \Gamma(\omega)$ (ω being the solvent viscosity). Escape occurs when the instantaneous position x of the particle reaches a critical value. It can be seen that when the particle momentum $p = mdx/dt$ and its acceleration term dp/dt is small (a situation occurring at large masses and high solvent viscosity), the acceleration term in the equation of motion can be excluded (overdamped regime). In this limit the probability to reach a critical amplitude (the rate) monotonously *decreases* as ω^{-1}. On the contrary, at low viscosity the Kramers theory predicts a turnover point, near this point the rate *increases* with ω (see Ref. 11). Recently this behavior has been confirmed by MD simulations.[12] The overdamping approximation can be safely applied (as we did) when studying the interaction between two nearby lipid bilayers because of their large mass and high solvent viscosity (equal or greater than water viscosity). Hence, we expect to observe a classical behavior where the adhesion/fusion rate decreases with viscosity.

The experimental and theoretical findings described above challenged us to look for a reasonable mechanism of the anomalous polymer effect on adhesion/fusion processes. Two possible scenarios could be envisaged:

(a) The polymer gyration radius R_g increases with polymer length N ($R_g \approx N^{3/5}$ for self-avoiding chains), hence attractive depletion forces (proportional to R_g^2 for large particles at short distance[13]) also increase. Therefore, weakly adhering vesicles remain in contact for a longer time, enabling the following fusion process. On the other hand, the increase of the polymer-related viscosity reduces the encounter frequency among freely diffusing vesicles. These competitive effects may lead to a maximum in the fusion rate.

(b) According to the above scenario, polymer modulates the number of vesicles pairs liable to fusion, while it does not modify the fusion probability of vesicles pairs. In order to prove this hypothesis we focused on a single vesicles pair instead, and we investigated the role of solvent viscosity on the vibrational dynamics of coupled membranes. We anticipate that viscosity behavior is more complex than expected, owing to the interplay among mechanical fluctuations, transport of the adsorbed ions along the membrane surface and bridging kinetics. Simply put, a first mechanism involves a coupling between mechanical oscillations and lateral fluctuations of adsorbed ions: at high viscosity membrane rigidity is low because of the relaxation of adsorbed ions during membrane oscillations. On the contrary, at low viscosity membrane rigidity is higher because the adsorbed ions cannot follow the fast membrane oscillations. Therefore, the encounter probability becomes smaller and smaller on *decreasing* solvent viscosity, provided membrane and ions relaxation rates are comparable (as for strongly adsorbed ions where the hopping rate is slow). Competition between the viscosity-modulated membrane rigidity and viscous damping might lead to a maximum in the plot of the encounter rate against viscosity ω. Another mechanism might explain the viscosity anomalous behavior. It relies on the competition between the viscosity-related decrease of membrane encounters and the longer lifetime of contact points that favour the bridging kinetics.

The formation of contact points among oscillating membrane represents the first event of the adhesion/fusion process. In a late time and under favourable conditions (e.g., in the presence of short-ranged stickers) membrane contact points may further evolve toward irreversible vesicles adhesion/fusion.

The dynamics of formation of inter-membrane contacts, as well as the effect of water-soluble uncharged polymers on membrane dynamics, will be the topic of the present study. In the first part of the paper we address the problem by a simplified non-equilibrium analytical model. In the second part of this work we report extensive coarse-grained MD simulations we had performed to validate our thoughts by a different and more realistic model of lipid membranes.

II. THEORY

The adhesion area of deformable lipid vesicles is large (the area increases with vesicles radius and adhesion strength,[14]) therefore, the planar geometry well simulates the adhesion region between large adhering vesicles or cells.

Consider two identical planar lipid bilayers, A and B, each of them bearing the same charge density σ and set at a mean distance $\bar{\ell}$ apart as shown in Fig. 1.

Bilayers may exchange ions with a large reservoir that contains an excess of monovalent anions and cations (typically $\sim 10^{-1}$ M NaCl in biological systems) together with a small amount of divalent cations.[15] Divalent cations (in biological systems mainly Ca^{++} but, to a less extent, also Mg^{++}) may form tight bonds with anionic lipid head groups. These ionic bonds are believed to be strong, as evidenced by binding studies[16] and MD simulations.[17]

Membranes are not rigid, they experience bending fluctuations that locally modify their relative distance. Letting $\eta_A \equiv \eta_A(x, y, t)$ and $\eta_B \equiv \eta_B(x, y, t)$ be the amplitude of instantaneous displacement from equilibrium, the local

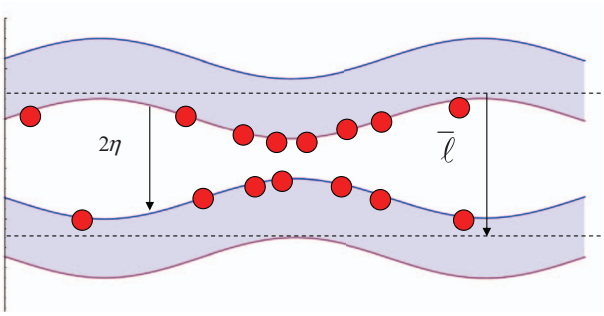

FIG. 1. Geometrical parameter used to describe two juxtaposed fluctuating bilayers. The red dots mimic divalent cations adsorbed onto the negatively charged surfaces of lipid bilayers. For clarity, adsorbed ions onto the external regions of the lipid bilayers have not been reported.

distance ℓ reads $\ell = \bar{\ell} - \eta_A \pm \eta_B$. The minus sign describes out-of-phase oscillations (squeezing modes) which lead to alternating patches of greater and shorter distances with respect to the mean distance $\bar{\ell}$. On the contrary, the plus sign describes in-phase pure bending modes where the relative distance does not change at each point of the membrane surface. In-phase oscillations are irrelevant to adhesion processes, the opposite happens when squeezing deformations are involved, in the following we will focus only on this kind of motion. Whence, considering two identical membranes, the local distance reads

$$\ell = \bar{\ell} - 2\eta(x, y, t). \tag{1a}$$

As said in the Introduction, charged membranes undergo short-range adhesion in the presence of divalent cations because of the following: (a) they form either *trans* complexes with two anionic lipids belonging to the same membrane or *cis* complexes with lipids belonging to juxtaposed membranes. *cis* complexes exist at the contact points alone, otherwise only *trans* complexes are present;[18] (b) formation of *cis* or *trans* complexes in negatively charged surfaces reduces the overall electrostatic repulsion.

The possibility to form tight ion-assisted bridges, together with a combination of repulsive and attractive forces at longer range, gives rise to a double energy minimum. Below a critical density of bridges-forming ligands (divalent cations), one usually observes only a shallow minimum at large interlamellar equilibrium distance (of order $\approx 2 - 4 \times 10^{-9}$ m). On increasing ligands concentration, a minimum at shorter distance (of order of the ligand molecular size) begins to develop. The energy minimum is stabilized by the strength of *cis* bridges.

Bound cations diffuse over the membrane surface. Experimental data suggest hindered hopping from one head of an anionic lipid to another (the lateral diffusion coefficient of the free calcium ions at infinite dilution and 25 °C is[19] $\approx 10^{-9}$ m^2 s^{-1}, while that of bound calcium is about one order of magnitude smaller.[20]) This latter result is also confirmed by our MD simulations reported in Sec. V B. Similar results have also been found for what concerns the proton mobility.[21] Even if these data probably overestimate the mobility of bound calcium because they refer to the average of free and bound ions lying near the membrane surface, we may conclude that ion mobility is severely reduced upon binding.

We define $\Theta_A \equiv \Theta_A(x, y, t)$ and $\Theta_B \equiv \Theta_B(x, y, t)$ be the local coverage degree of the membrane sites of *A* and *B* membranes. If we consider only the squeezing modes, the fluctuations of the surface coverage must follow distance fluctuations. In other words, any shortening (lengthening) of the membrane distance from equilibrium $\bar{\ell}$ must be accompanied by a corresponding increase (decrease) of the coverage. Thus, considering two identical membranes, at each point of the surface we impose $\Theta_A = \Theta_B \equiv \Theta$. Introducing the deviation with respect to the mean value $\overline{\Theta}$ we write down

$$\Theta = \overline{\Theta} + \theta(x, y, t). \tag{1b}$$

Notice the different sign between (1a) and (1b).

A. Bound ions-modified energy of interaction

The energy of interaction *per unit surface* between two planar juxtaposed membranes is modulated by the adsorption of ions that neutralize a fraction Θ of surface charges. Specifically, the energy is written as the sum of two contributions,

$$W_{interaction} = \int_S G_{electr}(\Theta, \ell) dS + \int_S G(\ell) dS. \tag{2}$$

The term $G_{electr}(\Theta, \ell)$ describes the electrostatic interactions. At low surface charge density the electrostatic energy reads $G_{electr}(\Theta, \ell) = 2\int_0^{\sigma_{eff}(\Theta)} \psi_{SURF}(\Theta, \ell) d\sigma \approx 2\frac{1}{2}\sigma_{eff}(\Theta)\psi_{SURF}(\Theta, \ell)$, where $\sigma_{eff}(\Theta)$ is the surface charge density and $\psi_{SURF}(\Theta, \ell)$ the surface potential (the factor 2 has been introduced because we are considering two identical membranes). The second term in Eq. (2), $G(\ell)$, describes other interactions that do not depend (or weakly depend) on surface charges (dispersion and hydration forces, as described in Sec. III). Also the osmotic forces related to the polymer addition to a lamellar system are incorporated into $G(\ell)$.

We let ρ be the surface lipid density (m^{-2}), e the unit charge of the anionic lipids, X the (charged lipids)/(total lipids) fraction, and $\sigma_{eff}(\Theta) = \rho e X(1 - Z\Theta) \equiv \sigma(1 - Z\Theta)$ the effective surface charge density. For the sake of simplicity, we assumed that each Z-valent cation (in most cases $Z = 2$) always neutralizes Z monovalent lipid heads, whence, the mean coverage $\overline{\Theta}$ is defined over the range $0 \le \overline{\Theta} \le 1/Z$. This is a convenient approximation, the error being negligible unless at very high ion concentration where a Z-valent ion could neutralize a number of charged lipids less than Z (charge reversal, a phenomenon sometimes observed, for instance, in calcium neutralization of clay lamellae or in multi-valent binding of charged polymers[22]).

The surface potential $\psi_{SURF}(\Theta, \ell)$ does depend upon the intermembrane distance ℓ and it has been approximated by the superposition of the potentials stemming from each of the two isolated, non-interacting membranes (the so-called Weak Overlap Approximation[23]),

$$\psi_{SURF}(\Theta, \ell) \approx \psi\ (\Theta)|_{\ell=0} + \psi(\Theta)|_{\ell=0}\, e^{-\kappa(\bar{\ell}-2\eta)}, \tag{3}$$

where $\psi\ (\Theta)|_{\ell=0}$ is the potential of the first membrane set at the origin $\ell = 0$ and, to a good approximation, $\psi(\Theta)|_{\ell=0} e^{-\kappa(\bar{\ell}-2\eta)}$ is the potential generated by the

other membrane set at a distance $\ell = \overline{\ell} - 2\eta$ apart. In Eq. (3) κ is the inverse of the Debye screening length $\kappa \equiv (4\pi e^2 \sum_i Z_i^2 \overline{c}_i / \varepsilon kT)^{1/2}$, with ε the solvent dielectric permittivity, e the ion charge, Z_i the valence of each ith ion in solution, and $\overline{c}_i$ its concentration in the bulk. The sum over the different ion species can be restricted to mono-valent ions alone because of their highest concentration in biological fluids, the role of divalent cations being negligible in modulating the Debye length.

The surface potential is related to the surface charge density $\sigma_{eff} = \sigma(1 - Z\Theta)$ through the standard boundary condition derived from electroneutrality condition $\varepsilon \frac{\partial \psi(\Theta)}{\partial \ell}|_{\ell=0} = 4\pi\sigma_{eff}$. In the case of small surface charge density $\psi(\Theta)|_{\ell=0} = \frac{4\pi\sigma}{\varepsilon\kappa}(1 - Z\Theta)$. The linear relationship between surface potential and charge density strictly applies to weakly charged membranes. The opposite high charge density limit is described in the Appendix. Combining the above results, we transform Eq. (2) as

$$W_{interaction} \approx \frac{4\pi\,\sigma^2}{\varepsilon\,\kappa} \int_S (1 - Z\Theta)^2 (1 + e^{-\kappa(\overline{\ell} - 2\eta)}) dS + \int_S G(\overline{\ell} - 2\eta) dS. \quad (4)$$

B. Energy of adsorbed and free ions

The energy of the adsorbed ions over the membrane plane can be approximated as

$$W_{ions}^{adsorbed} = 2\rho \int_S [kT(Z\,\Theta \log Z\Theta + (1 - Z\Theta)\log(1 - Z\Theta)) - E_{Adss} Z\Theta + wZ\Theta(1 - Z\Theta)] dS. \quad (5)$$

Again, we have counted twice the interactions because there are two membranes in the system. The first term, proportional to kT, represents the mixing entropy of an array of $Z\Theta$ occupied and $(1 - Z\Theta)$ vacant lipid heads. The second term, $-E_{Ads}Z\Theta$, describes the favourable interactions (per single bond) between adsorbed ions and membrane surface in the absence of electrostatic effects (e.g., interfacial solvation forces). Lastly, the third term in Eq. (5) accounts for the short-range interactions among occupied and vacant sites of the lipid membrane. When w is large and positive, the system shows a tendency to phase separate into domains richer in adsorbed cations, otherwise homogeneous mixing is favoured. Many experiments and simulations unambiguously proved the ability of divalent cations in triggering the formation of solid-like domains richer in calcium coexisting with fluid-like domains.[24] These results suggest large and positive values of w, due to the formation of extensive networks of anionic lipids connected through bridges-forming cations (*trans* complexes). In the following, however, we will consider only one-phase membranes by assuming that the combined effect of entropy and electrostatic repulsion is always greater than the lipid tendency to form thermodynamically stable phase-separated patches of lipids-ions coacervates.

To complete our analysis, we have to consider the energy of free ions. Let $\mathbf{N}$ be the total number of Z-valent ions in the system, and $N_{free} = \mathbf{N} - 2\rho\int_S Z\Theta dS$ be the number of unbound ions, the energy of free ions contains a solvation contribution, $-E_{free}$, plus an entropic term, $kT \log \overline{c}$,

$$W_{ions}^{free} = (-E_{free} + kT \log \overline{c})(\mathbf{N} - 2\rho \int_S Z\Theta dS). \quad (6)$$

C. Elastic energy

The elastic energy of two oscillating membranes is twice that of a single membrane. In the Helfrich approximation[25] it reads

$$W_{elastic} \approx 2\int_S \left[\tfrac{1}{2} K_M \left(\frac{\partial^2\eta}{\partial x^2} + \frac{\partial^2\eta}{\partial y^2} \right)^2 + K_G \left(\left(\frac{\partial^2\eta}{\partial x^2} \right) \left(\frac{\partial^2\eta}{\partial y^2} \right) - \left(\frac{\partial^2\eta}{\partial x \partial y} \right)^2 \right) \right] dS + 2\int_S \tfrac{1}{2}\gamma \left(\left(\frac{\partial\eta}{\partial x} \right)^2 + \left(\frac{\partial\eta}{\partial y} \right)^2 \right) dS, \quad (7)$$

where K_M is the bending rigidity per unit area and K_G is the elastic modulus of Gaussian curvature. Both K_M and K_G have been measured for a variety of lipid systems or they can be calculated by employing simple models. Typically $K_M \approx 10kT$, a value strongly depending on thickness, area per molecule, surface charge, temperature and impurities in the lipid bilayer.[25(b)] The last term in Eq. (7) describes the elastic contribution related to the membrane tension γ. For osmotically deflated flaccid vesicles γ is rather small,[26] while for tense vesicles the contribution of γ often dominates over K_M.[26]

The total free energy of the system is obtained by adding together the different energy contributions (Eqs. (4)–(7)),

$$W_{TOT} = W_{interaction} + W_{ions}^{Adsorbed} + W_{ions}^{free} + W_{elastic}. \quad (8)$$

Neglecting the fluctuation terms η and θ, minimization of the total free energy (8) with respect to the mean distance $\overline{\ell}$ and the mean ions coverage $\overline{\Theta}$ leads to a pair of coupled algebraic equations

$$\frac{Z\overline{\Theta}}{1 - Z\overline{\Theta}} = K_o \overline{c} \exp\left(\frac{\alpha}{\rho kT}(1 - Z\overline{\Theta})(1 + e^{-\kappa\overline{\ell}}) - \frac{w}{kT}(1 - 2Z\overline{\Theta}) \right), \quad (9a)$$

$$\frac{\partial G(\overline{\ell})}{\partial \overline{\ell}} = (1 - Z\overline{\Theta})^2 \alpha\kappa e^{-\kappa\overline{\ell}}, \quad (9b)$$

(with $0 \le \overline{\Theta} \le 1/Z$), where $\alpha \equiv 4\pi\frac{\sigma^2}{\varepsilon\kappa}$ and $K_o \equiv \exp((E_{Ads} - E_{free})/kT)$ is the intrinsic binding constant of the divalent cations adsorbed onto an isolated membrane at zero surface potential ($\alpha = 0$). From Eqs. (9a) and (9b)) the equilibrium values $\overline{\Theta}$ and $\overline{\ell}$ are numerically obtained. A typical example is shown in Fig. 2.

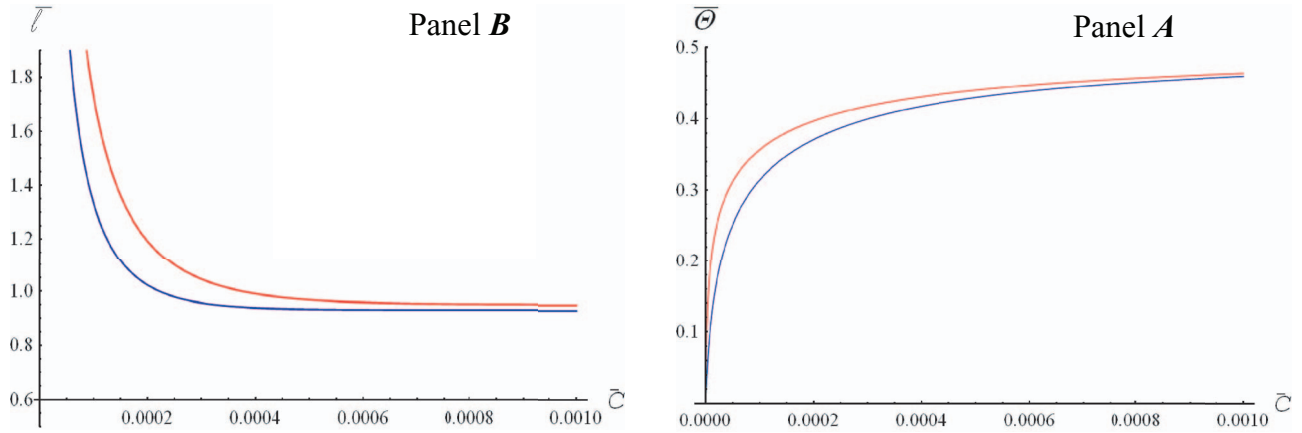

FIG. 2. (Panel a) Variation of the mean fraction of adsorbed divalent ions $\overline{\Theta} \leq 1/2$ against their concentration $\overline{c}$ (M) in the bulk phase. (Panel b) The corresponding variation of the inter-lamellar equilibrium distance $\overline{\ell}$ ($\times 10^{-9}$ m) with the bulk ions concentration $\overline{c}$.

Ideal mixing of the adsorbed ions was assumed ($w = 0$). Because the linearized Poisson-Boltzmann equation fails at high surface charge density we considered partially charged membrane surfaces in order to minimize the error. Red curves: membrane containing 30% of anionic lipids; Blue curves: membrane containing 20% of anionic lipids.

Two points are worth mentioning: (a) the slow increase of the fraction $\overline{\Theta}$ of adsorbed ions typical of anti-cooperative phenomena; (b) the decrease of the equilibrium inter-lamellar distance $\overline{\ell}$ with bulk ion concentration $\overline{C}$. Notice the unbinding transition at low surface charge neutralization (small $\overline{C}$) due to the overwhelming electrostatic repulsion.

D. Distance and concentration fluctuations

We proceed further by taking into account the effect of fluctuations. It is useful to look at a Fourier series expansion of the fluctuating variables θ and η,

$$\theta(\mathbf{r}, t) = \sum_q \theta_q(t) \cos(q_x x) \cos(q_y y),$$
$$\eta(\mathbf{r}, t) = \sum_q \eta_q(t) \cos(q_x x) \cos(q_y y). \tag{10}$$

(The choice of a cosinusoidal function reflects the symmetry with respect to the centre of mass of the oscillating lamellae. For laterally wide lamellae a sinusoidal or cosinusoidal description of membrane fluctuations merge to the same result, an exact calculation for finite lamellae requires the knowledge of the (unknown) boundary condition at the edge.) Inserting (10) into the total energy (8), the Fourier transformed energy becomes up to quadratic terms in θ and η,

$$W_{TOT}(q) = W^o_{TOT}(\overline{\ell}, \overline{\Theta}) + \tfrac{1}{4} S \sum_q [(K_M q^4 + \gamma q^2 + F_{11})|\eta_q(t)|^2 + 2F_{12}|\eta_q(t)\theta_q(t)| + F_{22}|\theta_q(t)|^2] \tag{11}$$

($q^2 \equiv q_x^2 + q_y^2$). In Eq. (11) $F_{11} \equiv 2\frac{\partial^2 G(\overline{\ell})}{\partial \overline{\ell}^2} + 2(1 - Z\overline{\Theta})^2 \alpha\kappa^2 e^{-\kappa\overline{\ell}} > 0$ measures the effective spring constant connecting two nearby oscillating membranes, while $F_{12} \equiv -2Z(1 - Z\overline{\Theta})\alpha\kappa e^{-\kappa\overline{\ell}}$ describes a coupling between membrane squeezing deformations and lateral fluctuations of adsorbed ions. Lastly, $F_{22} \equiv \frac{\rho kT}{\overline{\Theta}(1-Z\overline{\Theta})} - 2Z^2\rho w + Z^2\alpha(1 + e^{-\kappa\overline{\ell}})$ accounts for the energy of bound ions (if $F_{22} > 0$ the adsorbed ions lateral distribution is homogeneous, otherwise the system phase separates). Notice that the elastic modulus of Gaussian curvature K_G disappears in the transformed free energy. In order to calculate membrane dynamics, we introduce the transformed viscous dissipation,

$$\Im(q) = \tfrac{1}{4} S \sum_q \Gamma(\omega, q)|\dot{\eta}_q(t)|^2 \tag{12}$$

where $\dot{\eta}_q \equiv d\eta_q/dt$ and $\Gamma(\omega, q)$ is a friction coefficient proportional to solvent viscosity ω. Neglecting small inertial terms proportional to $\ddot{\eta}_q$ (the overdamped regime approximation, customarily employed in viscous fluids), we balance viscous and elastic forces to obtain an equation of motion

$$\frac{\partial \Im}{\partial \dot{\eta}_q} = -\frac{\partial W_{TOT}}{\partial \eta_q}. \tag{13}$$

Use of Eqs. (11)–(13) yields

$$-\Gamma(\omega, q)\dot{\eta}_q = (K_M q^4 + \gamma q^2 + F_{11})\eta_q + F_{12}\theta_q + R_q(t). \tag{14}$$

In writing Eq. (14) we added a random force, $R(\mathbf{r}, t)$, to describe the coupling with the surrounding heat bath. We assume $R(\mathbf{r}, t)$ to be a Gaussian white noise satisfying the time-averaging property $\langle R(\mathbf{r}, t)\rangle = 0$. The Fourier transformed random force is $R_q(t)$. Random forces play a key role in calculating the probability of forming contact sites. Stochastic differential equations, however, contain conceptual and mathematical difficulties as we shall see shortly and, as a rule, they are difficult to solve. Lastly, we have to define the friction coefficient $\Gamma(\omega, q)$. In the case of two coupled membranes, a Navier-Stokes based hydrodynamic model submitted to no-slip boundary conditions at membrane-water interface, gave a compact result,[27]

$$\Gamma(\omega, q) = 4\omega q \cdot B(x), \tag{15a}$$

where $q\bar{\ell} \equiv x$ and

$$B(x) \equiv \frac{1}{2}\begin{vmatrix} 1+\dfrac{x+\sinh x\cosh x}{\sinh^2 x - x^2} & -\dfrac{\sinh x + x\cosh x}{\sinh^2 x - x^2} \\ -\dfrac{\sinh x + x\cosh x}{\sinh^2 x - x^2} & 1+\dfrac{x+\sinh x\cosh x}{\sinh^2 x - x^2} \end{vmatrix}. \tag{15b}$$

Useful limits are

$$\Gamma(\omega, q) \approx \begin{cases} \dfrac{24\omega}{q^2\bar{\ell}^3} & q\bar{\ell} \ll 1 \\ 8\omega q & q\bar{\ell} \gg 1 \end{cases}. \tag{16}$$

Notice the different behavior at large and small wavelengths. As expected, the friction (16) is twice that occurring in a fluctuating membrane-solid substrate system[28] (a) different notation has been used in Ref. 28, Seifert's $\Gamma(\omega, q)$ is our $\Gamma^{-1}(\omega, q)$).

We need an additional equation to describe the lateral fluctuations of adsorbed ions onto the oscillating membranes plane. We start from the continuity equation by relating the flux of matter to the time evolution of local concentration: $\dot{\Theta} = -div\mathbf{J}$, where $div\mathbf{J}$ is the difference between the ingoing and outgoing flux of particles. In our quasi two-dimensional model, adsorbed ions migrate along the membrane surface through a hopping mechanism. Because of membranes oscillations, diffusion occurs along a curved surface.[29] It can be easily shown that curvature effects introduce non-linear terms disregarded in our model. Therefore, the motion of the adsorbed ions is restricted on the x-y plane. Accordingly, the continuity equation becomes: $\dot{\Theta} = -\frac{\partial J_x}{\partial x} - \frac{\partial J_y}{\partial y}$. Next, we relate the flux to the particles' velocity components v_i: $J_i = \Theta v_i$ ($i = x$ or y), and express v_i as a function of the thermodynamic force: $v_x = -\Lambda\partial\Phi/\partial x$ and: $v_y = -\Lambda\partial\Phi/\partial y$, where Λ is an Onsager mobility coefficient. The chemical potential Φ of the adsorbed ions is defined as $\Phi = \partial W_{TOT}/\partial n_{IONS} = (\partial W_{TOT}/\partial\Theta)(\partial\Theta/\partial n_{IONS})$, with $n_{IONS} = \rho S\Theta$ the number of adsorbed ions. Since $\Theta = \overline{\Theta} + \theta(x, y, t)$, we find $\Phi = (\rho S)^{-1}(\partial W_{TOT}/\partial\overline{\Theta} + \partial W_{TOT}/\partial\theta)$. At equilibrium $\partial W_{TOT}/\partial\overline{\Theta} = 0$ (this condition has been used to calculate the equilibrium concentration, Eq. (9a)), whence in the linear approximation,

$$-\dot{\theta}_q \approx \frac{q^2}{\rho S}\Lambda\overline{\Theta}\frac{\partial W_{TOT}(q)}{\partial\theta_q}. \tag{17}$$

At high coverage ($\Theta \to \frac{1}{Z}$), the mobility coefficient Λ of adsorbed ions must depend on the number of unoccupied binding sites $1 - Z\Theta$, falling to zero at full coverage. Thus,

$$\Lambda \approx \Lambda_o(1 - Z\overline{\Theta}). \tag{18}$$

An evaluation of Λ_o by MD simulations is given in Sec. V B. By combining Eqs. (11), (17), and (18), eventually we get a compact expression for the oscillation-modulated flux of adsorbed ions,

$$-\dot{\theta}_q = \beta(F_{22}\theta_q + F_{21}\eta_q), \tag{19}$$

where $\beta \equiv 2q^2\overline{\Theta}(1 - Z\overline{\Theta})\Lambda_o/\rho$.

Relationships (14) and (19) are the constitutive Langevin equations describing the coupled behavior of mechanical oscillations and facilitated diffusion of adsorbed ions. The motion is damped by viscous dissipation and is supported by random fluctuations of the heat bath.

Performing the change of variable: $t = \Gamma(q, \omega) \cdot \tau$, and introducing the ions diffusion coefficient at infinite dilution, $D_{ION} = \Lambda_o kT$, the Langevin equations (14) and (19) become

$$-\frac{\partial Y}{\partial\tau} = A_{11}Y + A_{12}X + R_q(\tau), \tag{20a}$$

$$-\frac{\partial X}{\partial\tau} = \Omega(A_{21}Y + A_{22}X), \tag{20b}$$

with $\eta_{\mathbf{q}}(\tau) \equiv Y$, $\theta_{\mathbf{q}}(\tau) \equiv X$, $A_{11} \equiv (K_M q^4 + \gamma q^2 + F_{11})$, $A_{12} \equiv F_{12}$, $A_{21} \equiv \rho F_{12}$, $A_{22} \equiv \rho F_{22}$, $\Omega \equiv \rho^{-1}\beta\Gamma(q, \omega)$.

E. Calculation of the encounter probability

From Eqs. (20a) and (20b) we derive a Fokker-Planck equation. It enables us to calculate the conditional probability $P_q(X, Y, t)$ of having at time t a given value of X and Y starting from some prescribed initial conditions. The resulting Fokker-Planck equation is easily obtained by standard methods[30] its solution is cumbersome. It should be more useful to separately discuss two relevant limiting cases.

1. High viscosity limit

In the high viscosity limit the ratio between the characteristic diffusion time of the adsorbed ions and the vibrational time of the interacting membranes is large. This ratio is described by a dimensionless coefficient Ω that, in terms of measurable parameters, takes a simple expression,

$$\Omega \equiv 8q^3\omega D_{ION}\frac{\overline{\Theta}(1 - Z\overline{\Theta})}{\rho^2 kT}B(q\bar{\ell}), \tag{21}$$

where $B(q\bar{\ell})$ has been defined by Eq. (15b). When $\Omega \gg 1$ we may set in Eq. (20b): $\frac{1}{\Omega}(\partial X/\partial\tau) \approx 0$. Solving Eq. (20b) for X, inserting the obtained result into Eq. (20a) and coming back to the original variable t, we obtain a standard one-dimensional Langevin equation: $\partial X/\partial t = C_q Y + R_q(t)$, with $C_q = \rho^{-1}(A_{11} - \frac{A_{12}A_{21}}{A_{22}})$ a constant independent of Y and t. The associated Fokker-Planck equation reads

$$\frac{\partial P_q}{\partial t} = D_o(\omega)\frac{\partial}{\partial Y}\left(\frac{\partial P_q}{\partial Y} + \frac{C_q}{kT}YP_q\right), \tag{22}$$

where $D_o(\omega) \equiv \rho kT/\Gamma(\omega, q) \propto \omega^{-1}$ measures the mobility of the vibrating membranes within the fluid (see Eq. (16). In the stationary case ($\partial P_q/\partial t = 0$), a first integral of Eq. (22) is

$$D_o(\omega)\left(\frac{\partial P_q}{\partial Y} + \frac{C_q}{\rho kT}YP_q\right) = -J_q \tag{23}$$

we may identify the integration constant $-J_q$ as the steady flux of vibrations going from Y to $Y + dY$ (hereafter we refer to J_q as the vibrational flux). A second integration gives

$$P_q(Y) = e^{-\frac{C_q Y^2}{2kT}}\left[-\frac{J_q}{D_o(\omega)}\int_0^Y e^{\frac{C_q Y'^2}{2kT}}dY' + I_q\right], \tag{24}$$

where I_q is another integration constant.

The stationary non-equilibrium probability P_q, so that an oscillation amplitude is comparable with the inter-lamellar distance $\bar{\ell}$, can be obtained from Eq. (24) once the integration constants J_q and I_q have been calculated by proper boundary conditions. They are as follows:

(a) we assume that the distribution of the smallest oscillations approaches the equilibrium one: $P_q^{equ}(Y) = P_o \exp\left(-C_q Y^2/2kT\right)$, where P_o is to be defined. P_o is found by imposing that the mass of a fluctuating membrane must be identical to its mass M at rest $\int_V P_q \rho dV = M$ ($M = \rho SL$, with ρ the membrane mass density, S its surface and L the thickness). In a fluctuating lamella $dV = SdY$ ($0 < Y < \bar{\ell}/2$, otherwise the juxtaposed membranes interpenetrate each other), then, integrating and solving for P_o, yields a first boundary condition,

$$\lim_{Y\to 0} P_q(Y) \approx L\left(\frac{2C_q}{\pi kT}\right)^{1/2} erf((C_q/8kT)^{1/2}\bar{\ell}) \tag{25a}$$

$erf(x)$ being the error function ($erf(x) \underset{x\gg 1}{\to} 1$, $erf(x) \underset{x\approx 0}{\to} (2/\pi)^{1/2}x$).

(b) A second boundary condition could be naively obtained by imposing that oscillations with an amplitude greater than a critical distance $2Y^* = \bar{\ell}$ are removed from the system (they evolve toward irreversible adhesion), namely, $P_q|_{Y=Y^*} = 0$. However, this approximation (often employed, for instance, in nucleation theories) grossly overestimates the capture rate of fluctuations. Indeed, as shown by us in a recent paper,[31] not all the vibrations reaching a critical contact distance are "adsorbed," most of them are reflected. Whence, it is more correct to assume that the flux of reactive oscillations is proportional to the (still unknown) probability $P_q|_{Y=Y^*}$ of having a fluctuation near the critical amplitude $Y = Y^*$. This is a classical radiation boundary condition often employed in diffusion problems, that is,

$$D_o(\omega)\left(\frac{\partial P_q}{\partial Y} + \frac{C_q}{kT} Y P_q\right)|_{Y=Y^*} = \xi \cdot P_q|_{Y=Y^*}, \tag{25b}$$

where the term in the left hand side represents the vibrational flux while $\xi(\mathrm{m\,s^{-1}})$ plays the role of an efficiency parameter. When $\xi \to \infty$ we recover the ideal adsorption condition $P_q|_{Y=Y^*} = 0$. We wonder about the meaning of ξ. Consider two fluctuating membranes meeting at an arbitrary point, this configuration is unstable, unless membranes are pinned together by tight short-range forces. A pinning mechanism, strong enough to preclude the following dissolution of a local protrusion, is the formation of cationic bridges among anionic lipids belonging to opposed bilayers (*cis* complexes). It is known that calcium ions may form either *trans* complexes with two anionic lipids belonging to the same membrane or *cis* complexes.[18] These findings suggest that ξ must depend on the probability p of having at the contact site both an adsorbed cation in a lipid bilayer and a vacant site on the juxtaposed bilayer: $p = Z\Theta(1 - Z\Theta)$. Furthermore, since the formation of a *cis* bridge at contact points requires a finite time, ξ must be also related to the contacts residence time. Since the lifetime is inversely related to the oscillation rate which, in turn, is inversely related to solvent viscosity ω, we write to the lowest approximation,

$$\xi \approx \xi_o(\Theta)\frac{\omega}{\omega_o}. \tag{26}$$

$\xi_o(\Theta) \propto Z\Theta(1 - Z\Theta)\xi^{ideal}$ being the efficiency parameter calculated in a solvent of viscosity ω_o (pure water). The dependence on other parameters, chiefly the stability energy of a *cis* bridge, is condensed into the empirical parameter ξ^{ideal}. The notions behind Eq. (26) are common to several contexts. For instance, they arise whenever a binding kinetics depends on a periodic force.[32] By applying the boundary conditions (25a) and (25b) and using Eq. (26), we calculated from Eq. (24) the integration constants J_q and I_q. Specifically, the flux J_q of vibrations reaching the contact distance reads

$$J_q = LD_o(\omega)\left(\frac{2C_q}{\pi kT}\right)^{1/2} \frac{erf((C_q/8kT)^{1/2}\bar{\ell})}{\frac{D_o(\omega)}{\xi(\omega)} e^{\frac{C_q\bar{\ell}^2}{8kT}} + \int_0^{\bar{\ell}/2} e^{\frac{C_qY'^2}{2kT}} dY'}. \tag{27}$$

For rigid lamellas ($C_q\bar{\ell}^2/8kT \gg 1$), where the encounter probability is low, asymptotic formulas $b\exp(-\frac{1}{2}b^2)\int_0^b \exp(\frac{1}{2}z^2)dz = 1 + O(b^{-2})$ and $erf(b) \underset{b\gg 1}{\to} 1 + O(\exp(-b^2))$ enable us to derive a simple relationship for the reactive vibrational flux (per unit surface) the high friction,

$$J_q^{high\ friction} = \frac{D_o(\omega)L}{\frac{D_o(\omega)}{\xi(\omega)} + (2kT/\bar{\ell}C_q)} \times (2C_q/\pi kT)^{1/2} e^{-C_q\bar{\ell}^2/8kT}. \tag{28}$$

Equation (28) depends on the wave-vector $\boldsymbol{q}$: vibrations of different wavelength have a different probability to generate contact sites. The next step is the averaging over $\boldsymbol{q}$. Assuming an uniform distribution of wave-vectors, using polar coordinate $q = (q_x^2 + q_y^2)^{1/2}$ and replacing the double summation by an integral: $\sum_{q_x}\sum_{q_y} \ldots \approx \frac{1}{(q^{MAX} - q^{MIN})^2/2} \int_{q^{MIN}/\sqrt{2}}^{q^{MAX}/\sqrt{2}} \ldots \cdot 2\pi q dq$, we find from Eq. (28)

$$\left\langle J_q^{high\ friction}\right\rangle \approx \frac{L}{2\pi\rho}\int_0^{2\pi\sqrt{\rho}} \frac{D_o(\omega)\cdot\left(2C_q^{relax}/\pi kT\right)^{1/2}}{\frac{D_o(\omega)}{\xi(\omega)} + \left(2kT/\bar{\ell}C_q^{relax}\right)} \times e^{-C_q^{relax}\bar{\ell}^2/8kT} q dq, \tag{29}$$

where, in deriving Eq. (29), we used the relationship: $q_j^{MIN} - q_j^{MAX} = 2\pi(\frac{1}{\sqrt{S_o}} - \frac{1}{\sqrt{S}}) \approx \frac{2\pi}{\sqrt{S_o}} \equiv 2\pi\sqrt{\rho}$, with S, S_o, and ρ the membrane surface area, that of a single lipid and the surface density, respectively. In writing Eq. (29) we introduced the super-script "relax" just to remember that the membrane-membrane interaction parameter C_q is calculated by allowing a full relaxation of adsorbed ions in the time course of mechanical

fluctuations,

$$C_q^{relax} \equiv \rho^{-1}\left(A_{11} - \frac{A_{12}A_{21}}{A_{22}}\right) = \frac{1}{\rho}\left[K_M q^4 + \gamma q^2 + 2\frac{\partial^2 G(\bar{\ell})}{\partial \bar{\ell}^2}\right] + 2(1 - Z\overline{\Theta})^2 \frac{\alpha}{\rho}\kappa^2 e^{-\kappa\bar{\ell}} - \frac{4Z^2\overline{\Theta}(1 - Z\overline{\Theta})^3 \frac{\alpha^2\kappa^2}{\rho^2 kT} e^{-2\kappa\bar{\ell}}}{1 + \frac{Z^2}{kT}\overline{\Theta}(1 - Z\overline{\Theta})\left(\frac{\alpha}{\rho}(1 + e^{-\kappa\bar{\ell}}) - 2w\right)}. \quad (30)$$

The last term in Eq. (30) describes the ion relaxation. This term is appreciable only for heavily charged membranes ($\alpha \gg 1$) and short inter-lamellar distances $\bar{\ell}$, vanishing both at $\overline{\Theta} = 0$ and $\overline{\Theta} = \frac{1}{Z}$ (either zero or full membrane coverage).

2. Low viscosity limit

In this latter limit, membrane oscillations are faster than the hopping diffusion of bound ions ($\Omega \ll 1$). As a consequence, the term $A_{12}X$contained in Eq. (20a) becomes extremely small. Neglecting this term, Eq. (20a) reduces to a standard Langevin equation for the random variable Y solvable using the same procedure employed in the high viscosity limit. The final equations are identical, the only difference being that a new coefficient, C_q^{frozen}, must replace the coefficient C_q^{relax} of Eq. (29),

$$\left\langle J_q^{low\ friction}\right\rangle \approx \frac{L}{2\pi\rho}\int_0^{2\pi\sqrt{\rho}} \frac{D_o(\omega)\cdot\left(2C_q^{frozen}/\pi kT\right)^{1/2}}{\frac{D_o(\omega)}{\xi(\omega)} + \left(2kT/\bar{\ell}C_q^{frozen}\right)} \times e^{-C_q^{frozen}\bar{\ell}^2/8kT} q\,dq, \quad (31)$$

where

$$C_q^{frozen} = \lim_{\omega\to 0} C_q^{relax} = \rho^{-1}A_{11} = \frac{1}{\rho}\left[K_M q^4 + \gamma q^2 + 2\frac{\partial^2 G(\bar{\ell})}{\partial \bar{\ell}^2}\right] + 2(1 - Z\overline{\Theta})^2\frac{\alpha}{\rho}\kappa^2 e^{-\kappa\bar{\ell}}. \quad (32)$$

The limiting expressions for C_q (C_q^{relax} (Eq. (30)) and C_q^{frozen} (Eq. (32))) evidence that C_q does depend on solvent viscosity ω. We interpolate these results to obtain an expression valid over the whole viscosity range. A satisfactory interpolation formula is

$$C_q(\omega) \approx \tfrac{1}{2}\left(C_q^{relax} + C_q^{frozen}\right) + \tfrac{1}{2}\left(C_q^{relax} - C_q^{frozen}\right) tgh \times [\lambda_q(\omega - \omega_{\max})], \quad (33)$$

where $tgh(x)$ is the hyperbolic tangent, λ_q is a decay rate, and $\omega_{\max}$ is the viscosity value at which the time scales of the membrane fluctuations and adsorbed ions diffusion are identical, their ratio, Ω, is given by Eq. (21). When the two time scales are identical we find from Eq. (21): $1 \equiv 4q^3\omega_{\max} D_{ION}\frac{\overline{\Theta}(1-Z\overline{\Theta})}{\rho^2 kT}B(q\bar{\ell})$ that can be solved for $\omega_{\max}$. Replacing Eq. (33) into Eq. (28), we obtain a unique expression for the reactive flux valid over the whole viscosity range,

$$\langle J_q(\omega)\rangle \approx \frac{L}{2\pi\rho}\int_0^{2\pi\sqrt{\rho}} \frac{D_o(\omega)\cdot(2C_q(\omega)/\pi kT)^{1/2}}{\frac{D_o(\omega)}{\xi(\omega)} + (2kT/\bar{\ell}C_q(\omega))} \times e^{-C_q(\omega)\bar{\ell}^2/8kT} q\,dq, \quad (34)$$

with $C_q(\omega)$ given by Eq. (33).

III. NUMERICAL CALCULATIONS

The numerical evaluation of our equations requires the knowledge of some parameters taken from the literature. Specifically, the bending elasticity modulus $K_M \approx 0.4 \times 10^{-19}$J $\approx 10kT$[25(b)] the thermal energy $kT = 0.4 \times 10^{-20}$ J at $T = 298\,^{\circ}$K, membrane tension $\gamma \approx 5 \times 10^{-2}$ J m^{-2},[26] the two-dimensional lipid membrane density $\rho \approx 10^{18}$ m^{-2},[16(a)] the bilayer thickness $L \approx 4 \times 10^{-9}$ m,[16(a)] the shortest bending fluctuations wavelength is the inverse of the lipid-lipid distance d: $q_{MAX} = 2\pi/d \approx \pi\sigma^{1/2} \approx 6 \times 10^9$ m^{-1}. In water and at physiological salt concentration, $\approx$0.1 M, the Debye length is $\kappa^{-1} \approx 10^{-9}$ m and the dielectric permittivity is $\varepsilon \approx 78$ (polymer chains are mostly excluded from the inter-lamellar space,[33] whence the dielectric permittivity of the membrane lumen approaches that of pure water). The solvent viscosity sharply increases with either polymer concentration or length. If we consider the commonly used PEG, solution viscosity goes from $\omega = 10^{-3}$ J m^{-3} s in pure water to values even two order of magnitude larger in 30%–40% PEG-containing aqueous solutions.[33]

Following the reasoning developed in Sec. II E, the parameter ξ, a measures of the efficiency of membrane encounters, has been expressed as a function of solvent viscosity as reported in Eq. (26). When $\xi \to \infty$ all the contacts above a critical distance evolve toward an irreversible adhesion/fusion event.

The force component per unit surface (pressure) between juxtaposed bilayers that does not depend on the electrostatic term has been decomposed as $P_{TOT} = -\partial G(\bar{\ell})/\partial\bar{\ell} = P_{hyd}(\bar{\ell}) + P_{vdW}(\bar{\ell}) + P_{osm}(\bar{\ell})$. The first term accounts for the hydration pressure $P_{hyd}(\bar{\ell}) \approx P(0)\exp(-\bar{\ell}/\lambda)$, typically:[34] $P(0) \approx 10^8$ J m^{-3}, $\bar{\lambda} \approx 2 \times 10^{-10}$ m, The van der Waals contribution reads $P_{vdW}(Z) \approx -\frac{H}{6\pi}\left(\frac{1}{\bar{\ell}^3} - \frac{2}{(\bar{\ell}+L)^3} + \frac{1}{(\bar{\ell}+2L)^3}\right)$, with the Hamaker constant $H \approx 10^{-20}$ J, and bilayer thickness $L \approx 5 \times 10^{-9}$ m. Lastly, in the case of planar lamellae embedded in a polymer-containing solution, the osmotic pressure behaves as $P_{osm}(\bar{\ell}) \approx -|const|$ if $\bar{\ell} < \ell_{crit}$ and $P_{osm}(\bar{\ell}) \approx 0$ if $\bar{\ell} > \ell_{crit}$ (ℓ_{crit} is proportional to the polymer gyration radius, while the constant term depends on polymer concentration). Osmotic forces enhance stability and lifetime of weakly adhering vesicles[1] and decrease their relative distance favouring fusion events, as theoretically,[3,35] and experimentally[36]

found. Here we do not explicitly consider the effect of the osmotic forces. Since the osmotic pressure is basically constant with the interlamellar distance, the only effect is a renormalization of the spacing $\overline{\lambda}$, that is $\overline{\lambda}$ is inversely related to polymer concentration. Other kinds of pressure generated by different mechanisms (e.g., the SNARE machinery in biological systems[37]) can be accounted for. Their most relevant effect is a reduction of the inter-lamellar distance $\overline{\ell}$, whence these forces can be included into an effective osmotic term $P_{osm}^{eff}(\overline{\ell})$. Nonetheless, in this work we neglected the term $P_{osm}^{eff}(\overline{\ell})$ because our focus is the viscosity and not the pressure effect. Consequently, the inter-lamellar distance was kept constant in all calculations, irrespective of polymer concentration. A few calculations performed by varying the inter-lamellar distance $\overline{\ell}$ with polymer concentration did not evidenced significant variations in the encounter probability.

A most effective and widespread fusogenic ion is calcium ($Z = 2$). The binding constant of calcium ion to negatively charged phosphatidylserine lipid bilayers is about $K_T \approx 0.5$–$30\ M^{-1}$, while either mono-valent cations or Mg^{2+} show significant lower figures.[16,17]

IV. RESULTS OF THE ANALYTICAL MODEL

Four relevant conclusions arise from our analytical model:

(a) Both at high and low friction, an increase of environmental viscosity ω should decrease the formation rate of contact points among fluctuating membranes. Although only a small fraction of contacts further evolves toward irreversible adhesion/fusion events, the greater the number of contact points, the higher the fusion rate is. These effects are accounted for by the pre-exponential term of Eqs. (29) and (31) through a viscosity-related coefficient $D_o(\omega) \approx \rho kT/\Gamma(q, \omega)$. Under the hypothesis that the encounters efficiency ξ parameter is independent of viscosity, the analytical behavior of the overall fusion rate as a function of ω is: $rate \approx (\omega + \frac{\cos t}{\xi})^{-1}$. This formula is practically indistinguishable from the empirical function: $rate \approx \omega^{-\alpha}$ $(0 < \alpha \leq 1)$ widely employed in the literature to fit viscosity data on chemical kinetics. A fractional exponent is typical of consecutive reactions with diffusion in sequence with a barrier crossing.[38]

(b) Besides the general viscosity behavior described at point (a), there are additional effects related to solvent friction. A first mechanism involves a coupling between mechanical oscillations and lateral fluctuations of adsorbed ions. A consequence of the coupling is an "apparent" decrease of membrane rigidity with friction: at high viscosity rigidity is low because of the relaxation of adsorbed ions during membrane oscillations. On the contrary, at low viscosity membrane rigidity could be higher because the adsorbed ions cannot follow the faster membrane oscillations. Therefore, the encounter probability becomes smaller and smaller on *decreasing* solvent viscosity, provided membrane and ions relaxation rates are comparable (as for strongly adsorbed ions where the hopping rate is slow). Competition between the viscosity-modulated membrane rigidity and viscous damping may lead to a maximum in the plot of the encounter rate against solvent viscosity ω.

(c) A second mechanism might explain the viscosity anomalous behavior. It relies on the competition between a viscosity-related decrease of membrane encounters and the longer lifetime of contact points that favour the bridging kinetics. This latter effect is described by the prefactor of the exponential term in Eq. (34) and it is effective also when the mechanism previously described at point (b) is negligible (i.e., $C_q(\omega) \rightarrow const$ independent of ω). In the limit $C_q(\omega) \rightarrow const$ Eq. (34) becomes

$$\left\langle J_q(\omega) \right\rangle \approx \int_0^{2\pi\sqrt{\rho}} \frac{A_1(q)\omega}{A_2(q) + \omega^2} q dq. \qquad (35)$$

Here $A_1(q)$ and $A_2(q)$ are two positive constants. That is, the rate behaves as the superposition of many q-depending functions, all of them showing a maximum at a certain value of ω.

The effects described at points (b) and (c) act in a synergistic way giving rise to the behaviour reported in Fig. 3 where we report the reactive flux of encounters (*rate* for short) against solvent viscosity ω for different values of the encounter efficiency parameter ξ^{max} (see Eq. (26)). An anomalous increase of the encounter rate at low viscosity, followed by the usual decay at high viscosity, is clearly observable.

(d) The plot of the membranes encounter rate against the bulk concentration $\overline{c}$ of divalent cations may show a skewed bell-shaped behavior. Results are summarized in Fig. 4. In spite of a fourfold viscosity increase (that should dramatically decrease the encounter rate), the formation of contact sites between fluctuating membranes is often larger in more viscous solvents (full line). This effect is sensitive to different parameters.

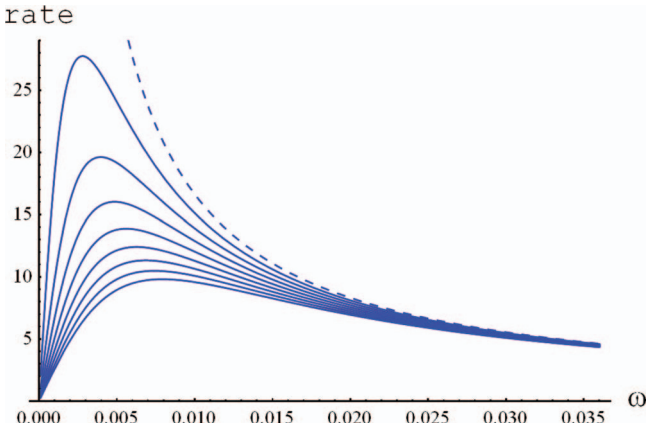

FIG. 3. Qualitative variation of the encounter probability rate ($\times 10^{-4}\ m\,s^{-1}$) against solvent viscosity ω ($J\,m^{-3}\,s$) calculated for different values of the encounter probability efficiency parameter ξ^{max}. From the top to the bottom: $\xi^{max}/\omega_o = 0.5,\ 1,\ 1.5,\ 2,\ 2.5,\ 3,\ 3.5,\ 4 \times 10^{-14}\ J^{-1}\ m^4\ s^{-2}$. Dashed line reports the ideal encounter rate calculated in the absence of adsorbed ions relaxation and assuming that all the encounters are reactive ($\xi^{max} \rightarrow \infty$). The interlamellar distance $\overline{\lambda}$ was assumed to be independent of polymer concentration, Calculations performed by assuming a decrease of $\overline{\lambda}$ with polymer concentration due to osmotic forces gave very similar results.

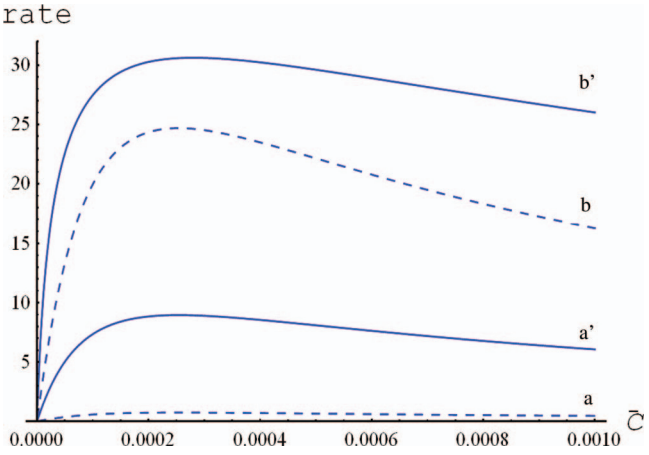

FIG. 4. Encounter probability rate between two fluctuating membranes ($\times 10^{-4}$ m s^{-1}) against the divalent ions concentration (M) in the bulk, for two different viscosity values. Dashed curve has been calculated using the viscosity of pure water ω_o, full curve has been obtained by using a fourfold more viscous solvent. The encounter probability efficiency parameter ξ^{max}/ω_o was set equal to 0.5 (curves a an b) and 5×10^{-14} J^{-1} m^4 s^{-2} (curves a′ and b′). Other parameters are as in Fig. 3.

Particularly relevant are the equilibrium inter-lamellar distance $\bar{\ell}$ and the non-ideal mixing parameter w/kT: short lamellar spacing and strong non-ideal mixing favour an anomalous viscosity behavior. At larger spacing, or nearly ideal mixing, the ions relaxation effect still persists, but it is overwhelmed by viscous damping.

Experimentally, the concentration behavior at low coverage has been widely investigated. Typically, the fusion rate is zero below a divalent ion concentration threshold, then it rapidly increases reaching a plateau. Thereafter, the rate decreases at high ion concentrations.[1(a)] Unfortunately, the high concentration region has been poorly investigated, nonetheless, a decrease of the fusion rate seems to be doubtless.

It is hazardous to compare our theoretical results with experimental findings on fusion rate. Our model calculate the frequency of contacts among fluctuating membranes, while experiments measure the number of *reactive* contacts that further evolve toward irreversible fusion. However, it is conceivable that the effect of solvent viscosity enters only in the preliminary steps (contact points formation). True fusion intermediates (stalk and connecting pore) involve full reorganization of the membrane inner core, so in the late stages lipid viscosity ω_L should play a more relevant role than solvent viscosity ($\omega_L \approx 10^3\omega$, see Ref. 39).

Despite its appealing simplicity, the model is basically qualitative in nature. Main flaws are: (a) the linearization of the differential equations, an approximation that may neglect significant physical phenomena; (b) the presence of several empirical parameters.

For this reason we undertook extensive Molecular Dynamics simulations in order to verify the correctness of our picture when applied to more realistic membrane models.

V. COMPUTATIONAL APPROACH

In this section we briefly describe Molecular Dynamics simulations performed to test whether: (a) the basic assumptions of the analytical model are correct; (b) the main predictions of the model are consistent with simulations. Main computational results will be reported in Sec. V B, while in Sec. V A we introduce the computational setup.

A. Coarse grained setup

The coarse-grained Martini parameterization[40] was used and the following systems were simulated:

(a) Two flat bilayers made up of 5304 molecules of negatively charged palmitoyl oleoyl phosphatidylglycerol (POPG). The bilayers were inserted in a water box (14 1917 water beads) in the presence of 0.1 M sodium chloride (5448 sodium ions, 824 chlorine ions). The solution contained also calcium ions 0.01 M (340 atoms) and 10% volume of inert uncharged polymer chains of PEG. The degree of polymerization N was 37. The solution was electroneutral.
(b) The same system as (a) but with an increased amount of PEG (30% volume fraction).
(c) The same system as (a) but without Calcium ions.
(d) The same system without PEG was used as a reference system (a).
(e-f) The results obtained from the above systems (a) and (d) with charged lipids were compared with those using neutral lipids. For that, we had a similar setup made up of neutral dipalmitoylphosphatidylcholine (DPPC). Water, PEG, and salt were added as above, except counterions.

The relative concentration ratio between the different species, in or outside the intermembrane space, has been determined from previous simulations described in Ref. 3. Here the system was consisting of the two membranes having free borders along the y-axis in order to allow for a flux of ions and PEG into and out of the inter-membrane space. For this, we constrained the lipids' centers of masses. After equilibrating the system for 500 ns, the density profiles of the species (ions and polymer) appear stabilized, in particular the intermembrane region appears depleted of PEG. Details about the forces involved in the polymer exclusion are discussed in Ref. 3.

Then we resized the box in order to have infinitive membranes, using periodic boundary conditions, and released constraints to allow fluctuations. For the first 100 ns we generated a pore to promote free diffusion of species for further equilibration. To this aim, lipid tails were made repelling each other in a cylindrically shaped region along the z-axis, following the mean field force approximation protocol as detailed in Risselada *et al.*[41] and shown in Fig. 5.

Recently the Martini group parameterized a new polarizable coarse-grained water model in order to reproduce the dielectric screening of bulk water.[42]

Because we are studying ion effects and charged lipids, we decided to switch to using the polarizable water model in order to benefit of a proper screening of interactions depending on the local environment. Therefore, all the systems (a–f) were rehydrated with polarizable water. We performed control simulations in order to verify the validity of our previous

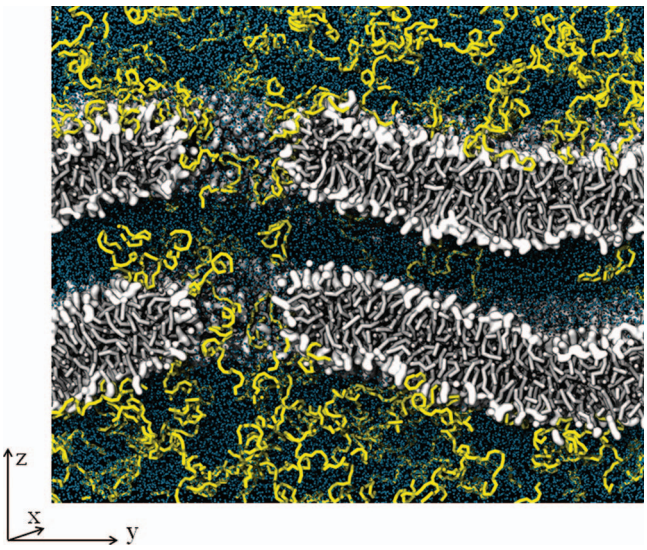

FIG. 5. An artificial pore crossing the two apposed membranes was generated to permit the diffusion of water (blue), ions (not represented), and polymer (yellow) through the membranes (tails in gray, headgroups in white).

observations for this system, and found that changing to the polarizable water model did not affect our results (data not reported). In several preparatory simulations we also tested the effect of different temperatures (300, 350, 400, 450, 500 K) to produce oscillations of appreciable amplitude. We decided to simulate all the systems at 450 K, to magnify the effect. At this temperature the interaction of PEG with the membrane is weak. After rehydration and slow heating to 450 K, each system was minimized by steepest descent and then equilibrated in NpT ensemble for 500 ns prior to data collection. After this period, indeed the density profiles of the species (ions and polymer) appear stabilized. The total simulation time was 1 μs for each of the systems.

Simulations were performed by version 4.5.4 of the GROMACS simulation package[43] and the MARTINI force field was used for DPPC lipids,[44] POPG lipids,[45] and PEG.[46] The Berendsen weak coupling temperature and pressure coupling algorithms[47] were utilized with coupling constants of 0.3 ps and 3.0 ps, respectively. Lipids, and water and ions were separately coupled to a heat bath. The Lennard-Jones potential was smoothly shifted to zero between 9 and 12 Å. For electrostatics, we used the Coulomb potential which was smoothly shifted to zero between 0 and 12 Å. The essence of CG

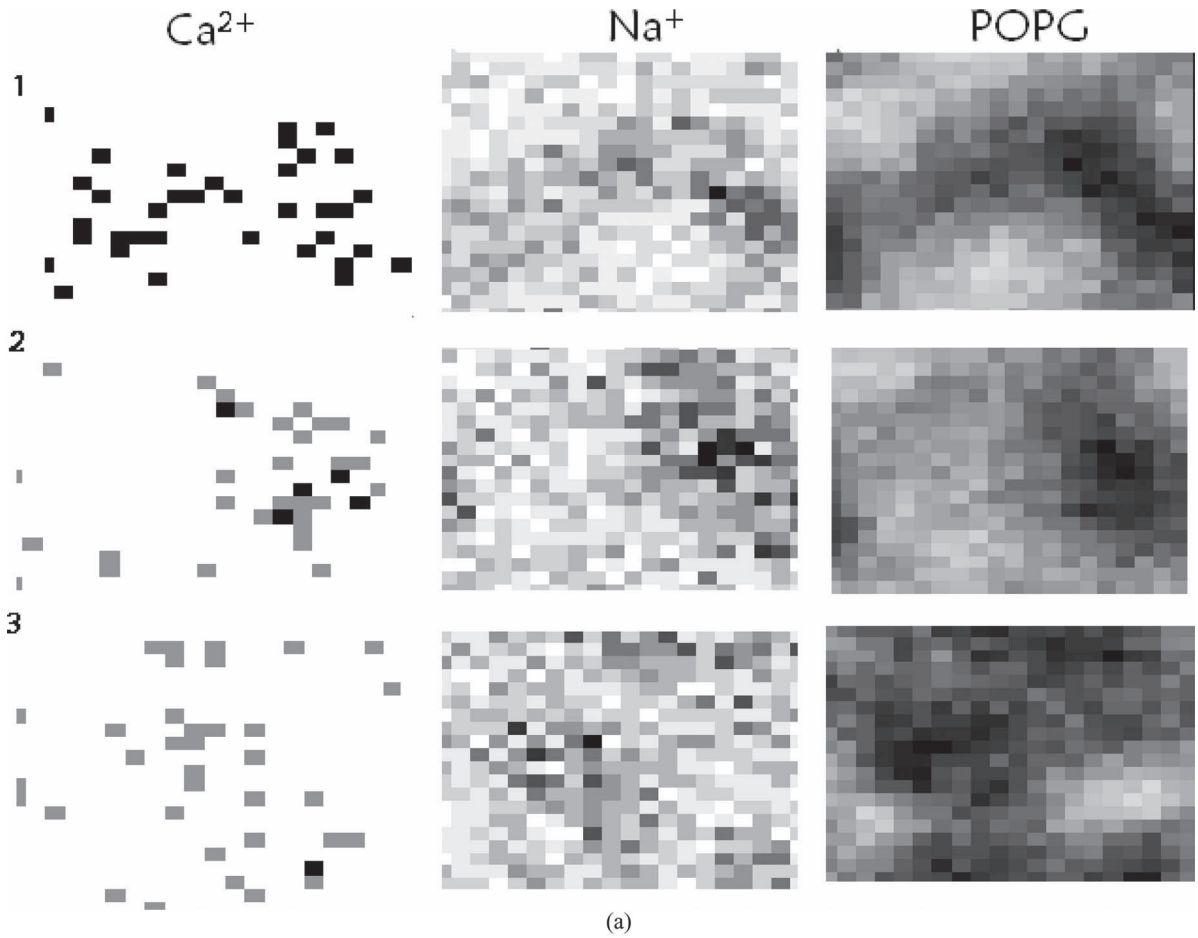

FIG. 6. (a) Qualitative profile of the densities of different species (sodium, calcium, POPG lipids) in the intermembrane region at different random timesteps. Upper panel: System in absence of PEG. Lower panel: System in presence of 10% of PEG. Fig. 6(b), upper panel: Average density of calcium, sodium, and POPG lipids along the last 200 ns of simulation in the intermembrane region in absence of PEG. (Lower panel) Average density of calcium, sodium and POPG lipids along the last 200 ns of simulation in the intermembrane region in presence of 10% of PEG. Fig. 6(c), upper panel: Average density of calcium, sodium, and DPPC lipids along the last 200 ns of simulation in the intermembrane region in absence of PEG. Lower panel: Average density of calcium, sodium, and DPPC lipids along the last 200 ns of simulation in the intermembrane region in presence of PEG.

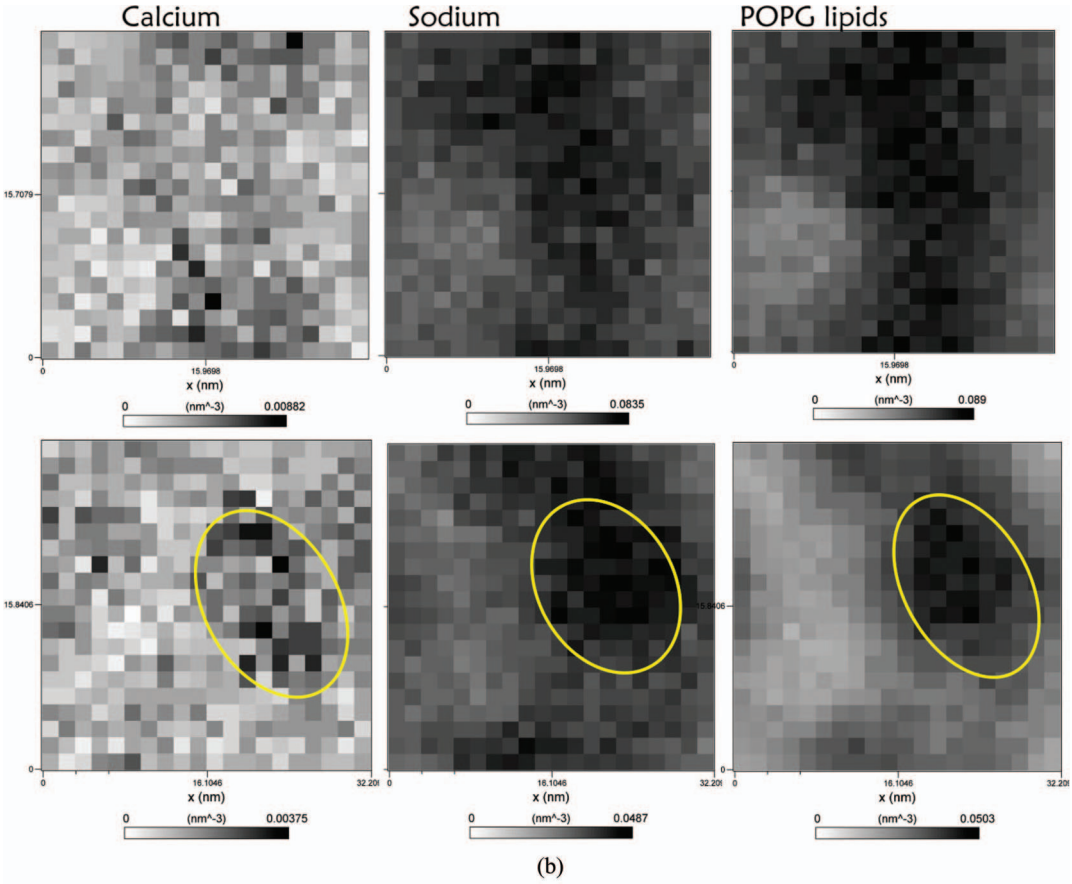

(b)

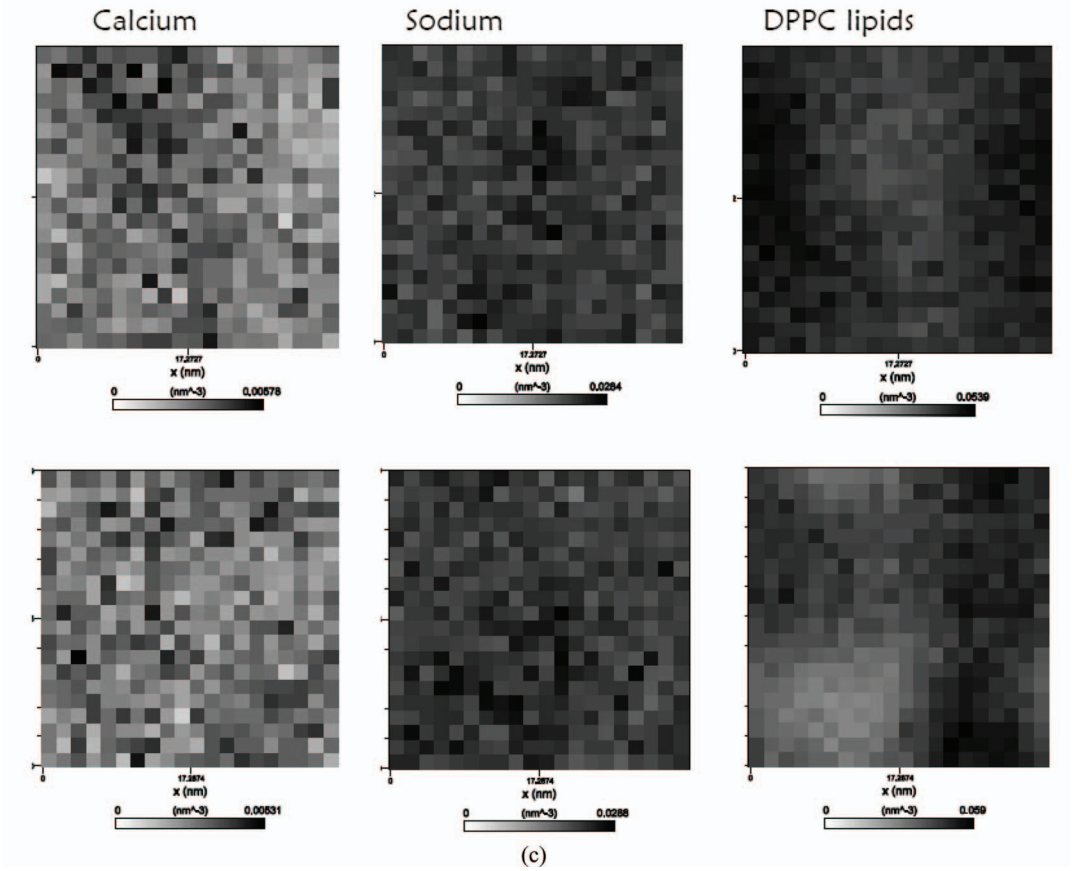

(c)

FIG. 6. *(Continued.)*

models is to use short-ranged potentials in order to be computationally efficient. This allowed us to explore cooperative effects of considerable entity like the exclusion of polymer from the inter-lamellar region between two hypothetical giant vesicles.[2,3] The time step was set to 0.025 ps when polymer was not present and to 0.010 ps for the system in presence of polymer.

B. Results of simulations

Our analytical model for calculating the formation rate of contact points between opposed fluctuating membranes relies on the coordinated fluctuations of distance and bridges-forming ions adsorbed on the membranes surface. To this aim, we first analyzed the geometrical features of our MD results to unveil the detailed adhesion mechanism. Specifically, we look at the density of the positively charged ions and lipids in the intermembrane region (distance between the headgroups belonging to opposite bilayers) at different random timeframes in presence or absence of PEG. Every time membranes become closer (higher density of lipids) there is a coherent accumulation of calcium and sodium ions (Fig. 6).

If we look at the total average density of negatively charged lipids, calcium and sodium ions along time (200 ns) in the intermembrane space, the trend emerges of membranes, in presence of PEG, to fluctuate in a limited region where contemporarily positively charged ions are more concentrated.

For the sake of comparison we report in Fig. 6(c) the behavior of neutral lipids (DPPC), calcium and sodium ions along time in the intermembrane space in presence or absence of PEG. The main evidence concerns the behavior of positively charged ions and lipids that, as expected, do not tend to fluctuate in a coherent way.

The contemporary increase of the ion density and decrease of the interlamellar distance is further highlighted by the snapshots shown in Fig. 7. Starting from two POPG membranes separated by a water layer measuring 4 nm, in presence of 10% PEG and calcium ions in the medium, we observe in Fig. 7 the formation of a contact zone on a time scale of 800 ns. Many calcium ions appear to be localized in proximity of the shorter intermembrane distance.

Taken together, our MD data show the *concerted* motion of mechanical oscillation and lateral fluctuation of adsorbed calcium ions ("calcium waves" for short). Next, we wonder if the MD simulations reproduce the anomalous viscosity behavior foreseen by our simple analytical model.

In Fig. 8 we report the number of contacts among two juxtaposed membranes vs time at different PEG concentrations.

MD results of Fig. 8 indicate that the polymer effect shows a maximum. Specifically, we observe that the encounter probability is extremely small without polymer, then it exhibits a maximum at intermediate (10%) polymer concentration (gray lines), tending to zero again at high (30%) PEG concentration.

Overall, this behavior is in very good agreement with that foreseen by our analytical model (see Figs. 3 and 4) where a maximum in the encounter rate was observed at intermediate values of solvent viscosity.

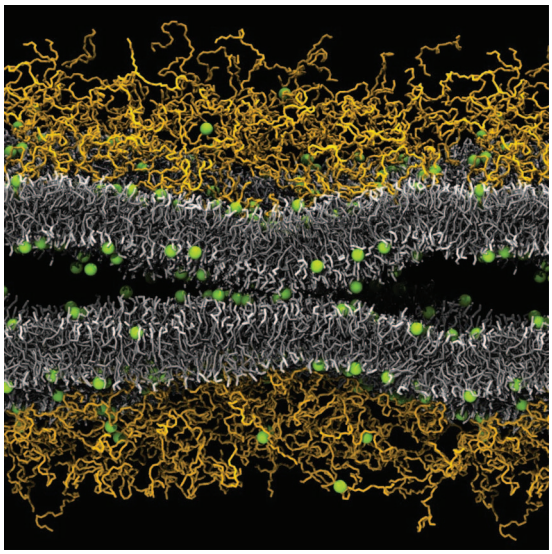

FIG. 7. Lateral section of POPG membranes (cyan beads) in presence of 10% of polymer (red beads) and calcium ions (0.01 M) (yellow beads) after 1 μs of simulation.

In addition, neutral membranes never interact (data not reported). Moreover, sporadic and short lifetime contacts are formed when the calcium is not included or in absence of PEG.

As it stands, the quite unexpected data reported in Fig. 8 do not explain the mechanism for the anomalous viscosity behavior. To this aim, a careful analysis of the time scales of the different processes is required.

According to classical hydrodynamics, viscosity should decrease the encounter rate by reducing the velocity of membrane fluctuations. The lowering of the averaged membrane velocity is inferred from our MD simulations through the

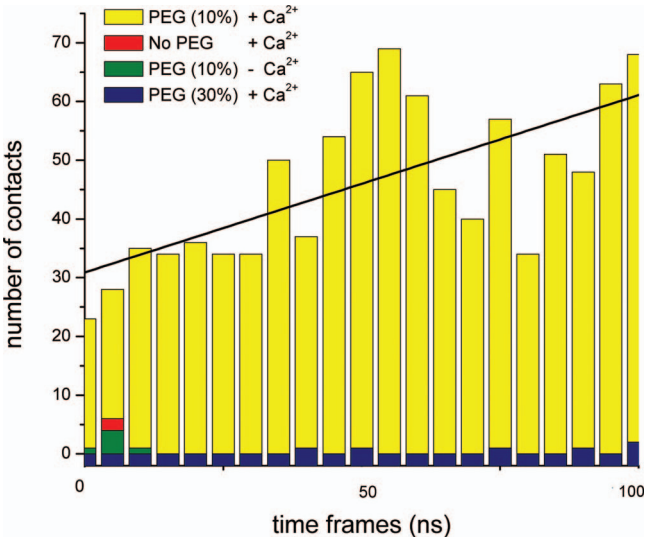

FIG. 8. Number of contacts after 700 ns of simulation between POPG membranes in presence of (a) 30% of PEG in blue (b) in presence of 10% of PEG and not calcium ions in green (c) in black in presence of 10% of PEG and Ca^{2+}, and (d) in red in presence of Ca^{2+} but not of PEG. Black linear fit is related to the system (b).

TABLE I. Diffusion coefficient (D) ($\times 10^{-9}$ m^2/s), at 450 K, of the POPG atoms in presence of different concentrations of polymer. D is calculated from the MSD along the z axis, using the g_msd analysis program of GROMACS, over 100 ns time periods using 40 different restarts. Due to the restricted diffusion of the lipids in the z-direction, the measure for D reflects the short time mobility rather than the long time diffusion rate.

System	D along the z-axis
POPG no PEG	0.008 +/− 0.003
POPG in presence of 10% of PEG	0.008 +/− 0.001
POPG in presence of 30% of PEG	0.004 +/− 0.001
DPPC no PEG	0.44 +/− 0.07
DPPC in presence of 10% of PEG	0.42 +/− 0.02

(short time) diffusion coefficient of the bilayer's atoms along the perpendicular z-axis. These data are reported in Table I.

The results from the MD simulations confirm the tendency of membranes to fluctuate slower in presence of PEG, as can be inferred from Table I.

While the polymer chains reduce the fluctuation rate of lipid membranes, it only slightly modifies the lateral diffusion of calcium and sodium ions along the membrane plane (Table II). Our results are consistent with several diffusivity[48] and conductance[49] measurements in bulk and at membrane surfaces.[50] These experimental data show only a modest obstruction-related effect of PEG on ion mobility. On the contrary, the diffusivity of calcium ions is about one-two orders of magnitude smaller than that measured in pure water[19] ($1.3 \times 10^{-9} m^2 s^{-1}$). The lowering of calcium diffusivity is due to strong ion-membrane interactions and it is consistent with experimental findings.[20,51] The difference between sodium and calcium diffusion coefficients ions reflects the different strength of binding with lipid headgroups.

The different viscosity behavior between membrane and ions mobilities depends on the ratio between the size of the diffusant and that of the polymer. The size of a fluctuating bilayer is much larger than the polymer gyration radius. Henceforth, membranes can be assimilated to macroscopic bodies and their dynamic behavior is well described by Stokes flow. On the contrary, the size of diffusing ions is much smaller than polymer gyration radius: ions freely diffuse through the polymer matrix, experiencing an effective viscosity similar to that of pure solvent.

Lastly, as shown in Table III, the time-averaged mean *amplitudes* of membrane oscillations remain comparable even at high PEG concentrations. Since the time-averaged amplitudes are independent of viscosity (equipartition theorem), our results confirm that PEG mainly affects the bilayer friction coefficient rather than its bending rigidity. This result is consistent with the mild PEG-lipid membrane interactions.

TABLE II. Diffusion coefficient (D) ($\times 10^{-9}$ m^2 s^{-1}), at 450 K, of calcium and sodium ions in the membrane plane. D was calculated over periods of 100 ns, using the g_msd analysis program of GROMACS with 40 different restarts.

	Ca^{2+}	Na^{+}
30% PEG	0.7 (+/− 0.1)	3.4 (+/− 0.02)
10% PEG	0.9 (+/− 0.05)	3.4 (+/− 0.03)
No PEG	0.95 (+/− 0.02)	3.8 (+/− 0.02)

TABLE III. Amplitude oscillations (angstroms) of POPG and DPPC membranes along the z-axis calculated at different viscosities.

	Amplitude oscillations	
System	Mean	Standard deviation
POPG − PEG	2.34	0.9
POPG + 10% PEG	2.29	0.8
POPG + 30% PEG	2.23	0.8
DPPC − PEG	2.26	0.8
DPPC + 10% PEG	2.26	0.8

By combining the results of Tables I–III, we are now in a position to understand the mechanism behind the anomalous viscosity behavior. Our data rule out an explanation based on a viscosity-induced transition from a "frozen" calcium lateral distribution at low viscosity to a "relaxed" distribution at high viscosity. Indeed, despite calcium ions are strongly bound to the negatively charged membrane surfaces and diffuse slower than in pure water, their diffusivity is always greater, on the average, than that of membrane oscillations (see Tables I and II). This means that ions always assume a "relaxed" distribution, both at low and high viscosities. A proof of this claim stems from the behavior of the intermembrane oscillations amplitudes reported in Table III. They remain strictly constant, irrespective of solvent viscosity (this is not true in a relaxed ions model).

Therefore, the only reasonable mechanism seems to rely on the competing effect between a viscosity-induced reduction of the membrane oscillations rate and the longer residence time of contact points that favors the formation of short range adhesion patches.

VI. CONCLUDING REMARKS

In conclusion, our combined analytical models and MD simulations unveil the subtle interplay between energetic and dynamic effects on the formation of ion-assisted adhesion patches in lipid membranes. Both methods have their own advantages and flaws. For instance, our linearized analytical model is simple and solvable. Unfortunately, linearization drops-off effects related to anharmonic terms, such as the mixing of normal modes. In this context MD simulations are far more realistic and unveil the detailed dynamics of the intermembrane distance and the lateral fluctuations of adsorbed calcium ions ("calcium waves") at different viscosities. However, the size and complexity of the system is huge (for what concerns both the number of particles and the simulation time), so reliable results require a great computational efforts and are affected by larger numerical errors.

Albeit still qualitative, our analytical and MD results highlight a strong *dynamic* coupling between local intermembrane distance and lateral concentration of adhesive species (stickers) on the membrane plane. The relative time scale of the coupled processes plays a key role and it can be tuned by varying the solvent viscosity. The proposed mechanisms

appear to be effective in a variety of soft matter systems with different time scales (related, e.g., to adhesion strength and molecular size). Applications will be described in future papers.

ACKNOWLEDGMENTS

Work partially supported by Italian Ministero Istruzione Università Ricerca. We would like to thank SARA (Amsterdam, the Netherlands) for computational resources.

APPENDIX: INTERACTIONS BETWEEN STRONGLY CHARGED MEMBRANES

The electrostatic equations developed in the main text strictly apply to weakly charged membranes. When the surface charge density $\sigma_{eff}(\Theta) = \rho eX(1 - Z\Theta)$ is large, the relationship between the surface potential $\psi(\Theta)|_{\ell=0}$ and $\sigma_{eff}(\Theta)$ differs from that obtained in the linear approximation, $\psi(\Theta)|_{\ell=0} = \frac{4\pi\sigma}{\varepsilon\kappa}(1 - Z\Theta)$, used in Sec. II A. Consider for simplicity a single charged bilayer embedded in a large excess of monovalent ions. Grahame equation[52] predicts that surface potential and density are related each other through a nonlinear relationship: $\sigma(1 - Z\Theta) = \sqrt{(2/\pi)\varepsilon\bar{c}_{TOT}kT}\sinh(\frac{e\psi(\Theta)|_{\ell=0}}{2kT})$ where $\bar{c}_{TOT}$ is the monovalent ion concentration. Also the electrostatic energy, $G_{electr}(\Theta)$, considerably differs from the simple result reported in Sec. II A for the linearized approximation: $G_{electr}(\Theta) \approx \frac{1}{2}\sigma_{eff}(\Theta)\psi_{SURF}(\Theta)$. Specifically, $G_{electr}(\Theta) = \frac{8\bar{c}_{TOT}kT}{\kappa}(\cosh(\frac{e\psi(\Theta)|_{\ell=0}}{2kT}) - 1)$. Combining the above results and recalling that for large X: $\cosh(X) \approx \sinh(X) \approx e^X$, we get in the limit of large surface charge density: $G_{electr} \approx const \cdot \sigma(1 - Z\Theta)$. This result has to be compared with that obtained in the opposite limit of low surface density $G_{electr} \approx const' \cdot \sigma^2(1 - Z\Theta)^2$ used by us in developing the model (see Eq. (4)). The above results can be improved by adding the effect of the second charged bilayer set an average distance $\bar{\ell}$ apart. We do not pursue this calculation since our goal was to show that the relationship between electrostatic energy and fraction of adsorbed ions Θ does not change its analytical structure both at high or low surface charge densities.

[1] For a review see, e.g., K. Arnold, in *Handbook of Biological Physics*, edited by R. Lipowsky and E. Sackmann (Elsevier, New York, 1995), Vol. I, pp. 903–957; B. R. Lentz, Eur. Biophys. J. **36**, 315 (2007).
[2] S. Asakura and F. Oosawa, J. Polym. Sci. **33**, 183 (1958).
[3] A. Raudino, M. Pannuzzo, and M. Karttunen, J. Chem. Phys. **136**, 055101 (2012).
[4] R. I. MacDonald, Biochemistry **24**, 4058 (1985).
[5] L. A. M. Rupert, J. B. F. N. Engberts, and D. Hoekstra, Biochemistry **27**, 8232 (1988).
[6] T. L. Kuhl, Y. Guo, J. L. Alderfer, A. D. Berman, D. Leckband, J. N. Israelachvili, and S. W. Hui, Langmuir **12**, 3003 (1996); T. L. Kuhl, A. D. Berman, S. W. Hui, and J. N. Israelachvili, Macromolecules **31**, 8258 (1998).
[7] M. Kurata and Y. Tsunashima, in *Polymer Handbook*, edited by J. Brandrup and E. H. Immergut (Wiley, New York, 1989).
[8] See, e.g., P. G. de Gennes, *Scaling Concepts in Polymer Physics* (Cornell University Press, Ithaca, NY, 1979).
[9] See, e.g., J. T. Hynes, J. Stat. Phys. **42**, 149–168 (1986).
[10] H. Risken, *The Fokker-Planck Equation* (Springer, Berlin, 1996).
[11] See, e.g., E. Pollak, *Dynamics of Molecules and Chemical Reactions*, edited by R. E. Wyatt and J. Z. H. Zhang (Dekker, New York, 1996), p. 617.
[12] J. Perkins, E. Edwards, R. Kleiv, and N. Weinberg, Mol. Phys. **109**, 1901 (2011).
[13] A. Hanke, E. Eisenriegler, and S. Dietrich, Phys. Rev. E **59**, 6853 (1999).
[14] U. Seifert and R. Lipowsky, *Morphology of Vesicles* (Elsevier, Amsterdam, 1995).
[15] S. Forsen and J. Kordel, "Calcium in biological systems," in *Bioinorganic Chemistry*, edited by I. Bertini (University Science Books, Michigan University, 1994), p. 107.
[16] (a) G. Cevc and D. Marsh, *Phospholipid Bilayers* (Wiley, New York 1985); (b) S. A. Tatulian, in *Phospholipid Handbook*, edited by G. Cevc (Dekker, New York, 1993), p. 511; (c) C. G. Sinn, M. Antonietti, and R. Dimova, Colloids Surf., A **282**, 410 (2006); (d) J. J. Garcia-Celma, L. Hataeht, W. Kunz, and K. Fendler, Langmuir **23**, 10074 (2007); (e) M. Sovago, G. W. H. Wurpel, M. Smits, M. Miller, and M. Bonn, J. Am. Chem. Soc. **129**, 11079 (2007).
[17] M. S. Miettinen, A. A. Gurtovenko, I. Vattulainen, and M. Karttunen, J. Phys. Chem. B **113**, 9226 (2009).
[18] G. W. Feigenson, Biochemistry **25**, 5819 (1986); G. W. Feigenson, **28**, 1270 (1989); J. E. Swanson and G. W. Feigenson, *ibid.* **29**, 8291 (1990).
[19] Y. H. Li and G. Sandra, Geochim. Cosmochim. Acta **38**, 703 (1974); A. C. F. Ribeiro, M. C. F. Barros, A. S. N. Teles, A. J. M. Valente, V. M. M. Lobo, A. J. F. N. Sobral, and M. A. Esteso, Electrochim. Acta **54**, 192 (2008).
[20] N. L. Allbritton, T. Meyer, and L. Stryer, Science **258**, 1812 (1992); N. F. Al-Baldawi and R. F. Abercrombie, Cell Calcium **17**, 422 (1995); M. Gabso, E. Neher, and M. E. Spira, Neuron **18**, 473 (1997); K. Nakatani, C. Chen, and Y. Koutalos, Biophys. J. **82**, 728 (2002).
[21] S. Serowy, S. M. Saparov, Y. N. Antonenko, W. Kozlovsky, V. Hagen, and P. Pohl, Biophys. J. **84**, 1031 (2003).
[22] Y. Murayama, Y. Sakamaki, and M. Sano, Phys. Rev. Lett., **90**, 018102 (2003); K. Besteman, K. Van Eijk, and S. G. Lemay, Nat. Phys. **3**, 641 (2007).
[23] J. N. Israelachvili, *Intermolecular and Surface Forces*, 3rd ed. (Academic Press, San Diego, 2011).
[24] J. R. Silvius, Biochemistry **29**, 2930 (1990).
[25] (a) W. Helfrich, Z. Naturforsch. **28**, 693 (1973); (b) for a recent analysis of membrane bending rigidity see, e.g., T. Baumgart, B. R. Capraro, C. Zhu, and S. L. Das, Annu. Rev. Phys. Chem. **62**, 483 (2011).
[26] E. Evans and W. Rawicz, Phys. Rev. Lett. **64**, 2094 (1990).
[27] M. Manghi and N. Destainville, Langmuir **26**, 4057 (2010), and references therein.
[28] U. Seifert, Phys. Rev. E **49**, 3124 (1994), a different notation has been used, Seifert's $\Gamma(\omega, q)$ is our $\Gamma^{-1}(\omega, q)$.
[29] E. Reister and U. Seifert, Europhys. Lett. **71**, 859 (2005); A. Naji and F. L. H. Brown, J. Chem. Phys. **126**, 235103 (2007).
[30] See, e.g., W. T. Coffey, Y. P. Kalmykov, and J. T. Waldron, *The Langevin Equation* (World Scientific, Singapore 2003).
[31] A. Raudino and M. Pannuzzo, J. Phys. Chem. B **114**, 15495 (2010).
[32] For a recent paper see, e.g., N. Gravish, M. Wilkinson, S. Sponberg, A. Parness, N. Esparza, D. Soto, T. Yamaguchi, M. Broide, M. Cutkosky, C. Creton, and K. Autumn, J. R. Soc., Interface **7**, 259 (2010).
[33] A. Raudino and M. Pannuzzo, J. Chem. Phys. **132**, 045103 (2010).
[34] See, e.g., H. I. Petrache, N. Gouliaev, S. Tristam-Nagle, R. Zhang, R. M. Suter, and J. F. Nagle, Phys. Rev. E **57**, 7014 (1998).
[35] J. Y. Lee and M. Schick, J. Chem. Phys. **127**, 075102 (2007).
[36] S. W. Burgess, T. J. McIntosh, and B. R. Lentz, Biochemistry **31**, 2653 (1992); J. Heuvingh, F. Pincet, and S. Cribier, Eur. Phys. J. E **14**, 269 (2004).
[37] *Molecular Mechanisms of Neurotransmitter Release*, edited by M. T. Palfreyman, E. M. Jorgensen, and Z.-W. Wang (Humana Press, 2008).
[38] R. M. Noyes, Prog. React. Kinet **1**, 129 (1961).
[39] B. D. Hughes, B. A. Pailthorpe, L. R. White, and W. H. Sawyer, Biophys. J. **37**, 673 (1982).
[40] S. J. Marrink, H. J. Risselada, S. Yefimov, D. P. Tieleman, and A. H. de Vries, J. Phys. Chem. B **111**, 7812 (2007).
[41] H. J. Risselada, A. E. Mark, and S. J. Marrink, J. Phys. Chem. B **112**, 7438 (2008).
[42] S. O. Yesylevskyy, L. V. Shafer, D. Sengupta, and S. J. Marrink, PLOS Comput. Biol. **6**, e1000810 (2010).

[43]B. Hess, C. Kutzner, D. van der Spoel, and E. Lindahl, J. Chem. Theory Comput. **4**, 435 (2008).
[44]S. J. Marrink, A. H. de Vries, and A. E. Mark, J. Phys. Chem. B **108**, 750–760 (2004).
[45]S. Baoukina , L. Monticelli, M. Amrein, and D. P. Tieleman, Biophys. J. **93**, 3775 (2007).
[46]H. Lee, A. H. de Vries, S. J. Marrink, and R. W. Pastor, J. Phys. Chem. B. **113**, 13186 (2009).
[47]H. J. C. Berendsen, J. P. M. Postma, W. F. van Gunsteren, A. DiNola, and J. R. Haak, J. Chem. Phys. **81**, 3684 (1984).
[48]F. Capuano, A. Vergara, L. Paduano, O. Annunziata, and R. Sartorio, J. Phys. Chem. B **107**, 12363 (2003).
[49]F. Capuano, G. Mangiapia, O. Ortona, G. d'Errico, and R. Sartorio, J. Solution Chem. **36**, 617 (2007).
[50]W. Guo, P. J. Photos, and T. K. Vanderlick, Ind. Eng. Chem. Res. **45**, 5512 (2006).
[51]S. Pöyry, T. Róg, M. Karttunen, and I. Vattulainen, J. Phys. Chem. B **113**, 15513 (2009).
[52]H.-J. Butt, K. Graf, and M. Kapp, *Physics and Chemistry of Interfaces* (Wiley-VCH, Weinheim, 2003).